

## Photoacclimation by Arctic Cryoconite Phototrophs

Perkins RG<sup>1\*</sup>, Bagshaw E<sup>1</sup>, Mol L<sup>2</sup>, Williamson CJ<sup>3</sup>, Fagan, D<sup>3</sup>, Gamble M<sup>3</sup> and Yallop ML<sup>3</sup>

1. Cold Climate Research, School of Earth and Ocean Sciences, Cardiff University, Park Place, Cardiff, UK, CF10 3AT

2. Department of Geography and Environmental Management, UWE Bristol, Coldharbour Lane, Bristol, UK, BS16 1QY

3. School of Biological Sciences, Life Sciences Building, University of Bristol, 24 Tyndall Avenue, BS8 1TQ

\*Corresponding author: Email: [PerkinsR@cf.ac.uk](mailto:PerkinsR@cf.ac.uk), Tel.: 0044 (0)2920 875026

### Abstract

Cryoconite is a matrix of sediment, biogenic polymer and a microbial community which resides on glacier surfaces. The phototrophic component of this community is well adapted to this extreme environment, including high light stress. Photoacclimation of the cryoconite phototrophic community on Longyearbreen, Svalbard was investigated using in situ variable chlorophyll fluorescence. Rapid light curves (RLCs) and induction recovery curves were used to analyse PSII quantum efficiency, relative electron transport rate and forms of down regulation including non-photochemical quenching (NPQ) including state transitions in cyanobacteria. Phototrophs used a combination of behavioural and physiological photochemical down regulation. Behavioural down regulation is hypothesised to incorporate chloroplast movement and cell or filament positioning within the sediment matrix in order to shade from high light, which resulted in a lack of saturation of RLCs and hence over-estimation of productivity. Physiological down regulation was biphasic NPQ: comprising a steadily induced light-dependent form and a light-independent NPQ that was not reversed

24 with decreasing light intensity. These findings demonstrate that cryoconite phototrophs  
25 combine multiple forms of physiological and behavioural down regulation to optimise light  
26 exposure and maximise photosynthetic productivity. This plasticity of photoacclimation  
27 enables them to survive productively in the high light stress environment on the ice surface.

28

29 Keywords: cryoconite, photoacclimation, down regulation, non-photochemical quenching,  
30 productivity, fluorescence

31

## 32 **Introduction**

33           Cryoconite (cryo = ice, conite = dust) is an important component of the glacier  
34 ecosystem. It consists of debris deposited on the ice surface by wind, water, or rockfall from  
35 valley sides, and collects in water-filled pools on the surface known as cryoconite holes. The  
36 debris contains microorganisms, including photoautotrophs, which contribute to the  
37 accumulation of carbon and bioavailable nutrients on glacier surfaces (Hodson *et al.* 2007;  
38 Cook *et al.* 2012; Bagshaw *et al.* 2016a). These nutrients are periodically exported to  
39 downstream environments via glacier runoff (Bagshaw *et al.* 2010; Lawson *et al.* 2014), and  
40 can support biological activity in proximal ecosystems (Foreman *et al.* 2004; Bagshaw *et al.*  
41 2013). Microorganisms in cryoconite are typically sourced from the surrounding  
42 environments, and include cyanobacteria, microalgae, archaea, bacteria, fungi and  
43 heterotrophic protists (Cameron *et al.* 2012; Edwards *et al.* 2014; Zawierucha *et al.* 2015;  
44 Kaczmarek *et al.* 2016). It is well-established that the photosynthetic organisms are active  
45 throughout the ablation season, but the mechanisms by which they undertake primary  
46 production on the harsh environment of the glacier surface are poorly understood. In this  
47 paper, we use in situ variable chlorophyll fluorescence to investigate cryoconite community  
48 photophysiology in order to gain insight into their adaptation to high light intensity, 24 h  
49 photoperiods (and hence the resulting high photodose) and rapid light intensity fluctuation.

50           Glacier surface microorganisms have been demonstrated to impact on ice surface  
51 albedo (Takeuchi 2002b; Yallop *et al.* 2012; Musilova *et al.* 2016), via a phenomenon known  
52 as ‘biological darkening’ (Benning *et al.*, 2014; Tedesco *et al.* 2016). In and ex situ studies  
53 have demonstrated that this occurs via two mechanisms: production of organic matter, which  
54 has a net darkening impact on the sediment (Takeuchi 2002a; Musilova *et al.* 2016), and  
55 production of dark pigments (Yallop *et al.* 2012; Lutz *et al.* 2014; Remias *et al.* 2016), which  
56 serve to protect photosynthetic apparatus from high light and/or UV (Dieser *et al.* 2010).

57 Yallop *et al.* (2012) demonstrated that highly pigmented populations of algae are widespread  
58 in marginal zones of the Greenland ice sheet, both concentrated in cryoconite, and living  
59 directly on the ice surface. Within cryoconite holes, the material aggregates into granules,  
60 forming a matrix of sediment particles and the microbial community, bound with biogenic  
61 extracellular polymers (EPS) (Hodson *et al.* 2010; Langford *et al.* 2010; Zarsky *et al.* 2013).  
62 These tightly-knit granules give structure to the cryoconite community, with heterotrophic  
63 organisms concentrated in the centre and phototrophs around the outside, which promotes  
64 community stability on the constantly changing glacier surface. During the summer months,  
65 cryoconite is regularly redistributed by flowing meltwater (Irvine-Fynn *et al.* 2011), hence  
66 granule formation may be an adaptation to promote community longevity (Bagshaw *et al.*  
67 2016b).

68 To our knowledge there have been very limited in situ measurements of microbial  
69 phototrophs in ice/snow-associated communities, presumably due to the difficulty in  
70 collecting data in these harsh environments. McMinn *et al.* (2007) used variable chlorophyll  
71 fluorescence to perform measurements on ex situ samples of Antarctic sea ice algae. Stibal *et al.*  
72 (2007) used in situ variable chlorophyll fluorescence to measure snow algae, however  
73 these samples were thawed and analysed in a cuvette system. Yallop *et al.* (2012)  
74 investigated ice algal photophysiology and their role in reducing ice sheet albedo, but  
75 samples were analysed ex situ after thawing. Bagshaw *et al.* (2016) made a comparative  
76 study of Arctic and Antarctic cryoconite using combined oxymetry and fluorescence, also on  
77 ex situ cryoconite material in a cuvette system. By contrast, this is the first study of  
78 cryoconite phototroph photophysiology in situ. We use a Walz Water PAM fluorometer with  
79 fibre optic emitter-detector to perform in situ rapid light response curves and induction  
80 recovery curves in cryoconite holes on Longyearbreen, Svalbard, in order to understand the

81 role of photophysiological down regulation in optimising primary production in this extreme  
82 environment.

83

## 84 **Methods**

### 85 *In situ field measurements and sampling*

86 Field work was carried out at Longyearbreen, Svalbard (78° 10 49 N, 15°30 21 E) in the  
87 high-Arctic, on 25-30<sup>th</sup> August 2015. Longyearbreen is a small (2.5km<sup>2</sup>), thin (53m,  
88 (Langford *et al.*, 2014)), predominantly cold-based valley glacier, adjacent to the town of  
89 Longyearbyen, surrounded by Tertiary and Cretaceous sandstone (Larsson 1982) interbedded  
90 with coal-bearing shales and siltstones (Langford *et al.* 2014). Field observations indicate that  
91 sediment production is driven by frost shattering of the bedrock and glacial action. This  
92 material is moved onto the glacier surface through aeolian deposition and high frequency  
93 rock falls (Etzelmüller *et al.* 2011).

94         Sampling was undertaken near the centre line of the glacier (Figure 1), which had  
95 relatively high debris concentrations including a small morainic deposit. Three hydrologically  
96 connected cryoconite holes were chosen at random within 10 m<sup>2</sup> at 78°10.903 N, 15°31.469  
97 E, for in situ measurements and sample collection for identification of the photosynthetic  
98 community structure using microscopy and pigment analysis. Sediment depth was 4-6 mm  
99 and water depth was 10-15 mm in the three holes.

100         Bulk samples of cryoconite from each hole were collected immediately after  
101 fluorescence measurements were made (see below), using new nitrile gloves and Whirlpak  
102 sterile sampling bags (Fisher Scientific). They were frozen within 4 hours of collection, and  
103 transported frozen in insulated boxes to Cardiff University, UK. Samples for initial  
104 microscopy were scraped from the debris or ice surface using an ethanol-sterilised knife or

105 spatula, and transferred to new centrifuge tubes. They were returned to the field laboratory,  
106 kept cool and examined within 48 hours. During the short sampling period, incoming  
107 photosynthetically available radiation (PAR) and water temperature of an example cryoconite  
108 hole in the sampling area were monitored using an Apogee Quantum sensor and Campbell  
109 Scientific 107 probe, powered by a Campbell Scientific CR10X datalogger.

110           In situ variable chlorophyll fluorescence measurements were made using a Walz  
111 Water Pulse Amplitude Modulated (PAM) fluorometer equipped with a blue light fibre-optic  
112 emitter/detector unit. This instrument measures emitted fluorescence yield for calculation of  
113 photosystem II (PSII) quantum efficiency, which in turn can be used to calculate relative  
114 electron transport rate as a proxy for photophysiological productivity. Measurements  
115 consisted of 10 rapid light curves (RLCs) and 5 induction-recovery curves within each  
116 cryoconite hole, carried out over the same time period each day, between approximately  
117 10:00 and 18:00 when solar irradiance was high. The photoperiod at the time of sampling in  
118 August 2015 was 20 h. Initially three measurements of RLCs were made with a blue or a red  
119 light emitter/detector unit to investigate the relative excitation of microalgae and  
120 cyanobacteria respectively (this was prior to identification of taxa present, however  
121 cyanobacteria were expected based on previous work and literature). However, no significant  
122 difference was observed between the two systems and therefore measurements were only  
123 made with one, the blue light emitter/detector unit. RLCs were in two forms: increasing and  
124 decreasing incremental light steps, with 5 replicates of each, following the methods of  
125 Perkins *et al.* (2006). Increasing and decreasing light curves were carried out on separate  
126 samples each time and with sequentially increasing or decreasing light levels steps  
127 respectively. Increasing eight-step RLCs were carried out using 30 second incremental light  
128 steps between 0 and 3,600  $\mu\text{mol m}^{-2} \text{s}^{-1}$  photosynthetic available radiation (PAR). A 600 mS  
129 saturating pulse at intensity setting 10 (in excess of 8,000  $\mu\text{mol m}^{-2} \text{s}^{-1}$  PAR) was observed to

130 induce full light saturation and rise to maximum fluorescence yield ( $F_m$  or  $F_m'$ ). The  
131 increasing incremental light curves were randomly interspersed with 5 replicates of  
132 decreasing incremental light curves. For these light curves, instead of using the pre-  
133 programmed RLC settings of the fluorometer, manual light curves were performed,  
134 decreasing the light intensity each step using Walz WinControl V3.14 software. At the end  
135 of each light curve step a saturating pulse was performed and the light level reduced to the  
136 next lower intensity, culminating in a 30 second dark period measurement. Rapid light curves  
137 of relative electron transport rate (rETR) as a function of incremental light intensity were  
138 plotted, with rETR calculated as:-

$$139 \quad \text{rETR} = \text{quantum efficiency } (\Delta F/F_m') \times \text{PAR}/2$$

140 where  $\Delta F/F_m'$  is the quantum efficiency calculated as  $(F_m' - F)/F_m'$  and where  $F$  is the  
141 operational fluorescence yield and  $F_m'$  is the maximum fluorescence yield in the light and  $\Delta F$   
142  $= F_m' - F$ . RLC data were analysed by iterative curve fitting of the Eilers and Peeters (1988)  
143 model using Sigmaplot V10 statistical software. Light curves data were solved to determine  
144 the RLC parameters of relative maximum electron transport rate (rETR<sub>max</sub>), light utilisation  
145 coefficient ( $\alpha$ ), and light saturation coefficients ( $E_s$  and  $E_k$ ). Light curve coefficients a, b and  
146 c and the regression fit for the light curves were all observed to be significant at  $p < 0.001$   
147 ensuring accuracy in calculation of the light curve parameters (Perkins *et al.* 2006).  
148 Parameters rETR<sub>max</sub>,  $\alpha$ ,  $E_k$  and  $E_s$  were analysed for equal variance and normality using the  
149 Levene's and Shapiro Wilkes tests respectively in PAST statistical software (Hammer *et al.*,  
150 2001). Data were homoscedastic and parametric; two factor ANOVA was used to  
151 determine significant differences between the three cryoconite holes and between increasing  
152 and decreasing RLCs. RLC *in situ* measurements were performed randomly between the  
153 three cryoconite holes over two days, with induction recovery curves performed the  
154 following day. Again, 5 sets of measurements were performed for each cryoconite hole.

155 Induction recovery curves consisted of an initial dark measurement (30 seconds of darkness)  
156 of quantum efficiency ( $F_v/F_m$ ), followed by a 400 second induction phase of applied actinic  
157 light at  $803 \mu\text{mol m}^{-2} \text{s}^{-1}$  PAR, with repeated recording of quantum efficiency ( $\Delta F/F_m'$ ). This  
158 was then followed by the recovery phase of a further 900 seconds of darkness, with repeated  
159 measurement of quantum efficiency ( $F_v/F_m$ ). Changes in quantum yield and fluorescence  
160 yields (operational fluorescence yield  $F$ , and maximum fluorescence yields  $F_m$  and  $F_m'$ ) were  
161 analysed over the full induction-recovery period.

### 162 *Community analysis*

163 Cells in cryoconite subsamples were identified using a Leica DM LB2 light  
164 microscope with fluorescence attachment. For pigment quantification, subsamples of  
165 cryoconite material, frozen ( $-20^\circ\text{C}$ ) were freeze-dried and homogenised prior to the extraction  
166 of a known mass (circa 2 g) and pigments were extracted in 100% acetone containing vitamin  
167 E as the internal standard. The HPLC protocol was a modified version of the method of Van  
168 Heukelem & Thomas (2001), using a c8 column in an Agilent 1100 HPLC equipped with a  
169 diode-array detector. Pigments were identified and quantified against analytical standards  
170 from DHI and Sigma using both retention time and spectral analysis.

171

### 172 **Results**

173 Ambient photosynthetically available radiation (PAR) received on the glacier surface ranged  
174 from 200 to  $400 \mu\text{mol m}^{-2} \text{s}^{-1}$  (st dev. 18) during the measurement period. The mean water  
175 temperature in the monitored cryoconite hole was  $0.9^\circ\text{C}$ , and ranged from  $0.4$  to  $1.9^\circ\text{C}$ . The  
176 sampled holes remained hydrologically connected throughout the monitoring period,  
177 although the degree of connection varied diurnally. The sediment layers remained intact,



178 nonetheless mobile sediment particles were observed moving across the ice surface in the  
179 meltwater (Irvine-Fynn *et al.*, 2011).

#### 180 *Cryoconite phototrophic community composition*

181 Epifluorescence microscopy on cryoconite material revealed the presence of a number  
182 of different green algal and cyanobacterial taxa in the three different cryoconite holes  
183 sampled (Table 1). Large colonies of *Nostoc* spp. (Figure 2a) and Streptophytes (closely  
184 related to Charophyceae and Embryophyta), were identified in samples from all three holes.  
185 Pigments characterising both green algae and cyanobacteria were recorded from the  
186 cryoconite material using HPLC (Table 2). Chlorophyll *a* (CHL *a*) pigment dominated all  
187 samples, but was higher in hole 1 than holes 2 and 3. Hole 1 also had the highest  
188 concentrations of the pigments lutein (LUT), chlorophyll *b* (CHL *b*) and echinenone (ECHI).  
189 The ratios of Lutein and CHL*b* : CHL *a* (Table 3) were 2-6 times greater than in the other  
190 samples, indicating that green algae dominated the community in this hole. There were two  
191 key cyanobacterial markers, echinenone (ECHI) and canthaxanthin (CANT) present in all  
192 samples from the three cryoconite holes. The orange-brown pigment Scytonemin (present in  
193 the sheath of *Nostoc* (Figure 2a)) was found in all samples though it could not be quantified  
194 due to poor resolution of the peaks. Although occasional spores of *Chlamydomonas* spp. were  
195 found (Figure 2c), the red pigment astaxanthin was below the detection limit in pigment  
196 extracts. Detectable levels of fucoxanthin in holes 1 and 3, indicated that diatoms were also  
197 present. Differences in the ratios of pigment markers between holes indicated differences in  
198 relative abundance of taxa, with relatively more cyanobacteria in hole 1.

#### 199 *Cryoconite phototrophic community photophysiology*

200 Increasing rapid light curves (RLCs) showed virtually no saturation (Figure 3), with  
201 14 of 15 curves failing to saturate, and one single curve approaching saturation. As a result,

202 rETR<sub>max</sub> could only be estimated as the highest value obtained ( $255 \pm 37.2$  rel. units). In  
203 contrast, decreasing RLCs (Figure 3) showed clear saturation, with all 15 curves saturating  
204 and an rETR<sub>max</sub> of 113 rel. units ( $F_{2,10} = 551$ ,  $p < 0.001$ ). Hence, rETR<sub>max</sub> determined from  
205 decreasing RLCs was less than 50% of the value estimated from the non-saturating,  
206 increasing RLCs. Examination of both sets of RLCs showed no significant difference in the  
207 light saturation coefficient ( $\alpha$ ), with values of 0.13 (increasing) and 0.12 (decreasing) rel.  
208 units. For decreasing RLCs, an  $E_k$  of 940 and  $E_s$  of 1800  $\mu\text{mol m}^{-2} \text{s}^{-1}$  PAR, were determined.

209         Calculated down regulation in the form of non-photochemical quenching (NPQ) was  
210 notably different between increasing and decreasing RLCs (Figure 4); note that calculated  
211 values do not correct for NPQ retained from the period prior to measurements, i.e. induced  
212 under ambient light. For decreasing RLCs there was no initial dark light curve step, and  
213 hence no reversal of any NPQ that had been induced under ambient light prior to the  
214 measurement period. Whilst NPQ slowly increased with PAR from  $0$  to  $0.50 \pm 0.06$  during  
215 increasing RLCs, an inverse relationship between NPQ and PAR was apparent during  
216 decreasing curves: as light levels were stepped down from 3505 to approximately 800  $\mu\text{mol}$   
217  $\text{m}^{-2} \text{s}^{-1}$  PAR, NPQ slowly increased. With further reductions in PAR, NPQ rapidly increased  
218 to approximately 6-times that induced during increasing RLCs. These high levels of NPQ  
219 were further retained in the dark during the final 30 second step of decreasing RLCs.

220         Examination of RLC fluorescence yields revealed the dynamics underlying observed  
221 differences in down regulation between increasing and decreasing RLCs (Figure 5). During  
222 increasing RLCs (Figure 5a), initial increases in both  $F$  and  $F_m'$  signified reversal of NPQ  
223 retained from illumination of samples by ambient light prior to measurements: such retained  
224 NPQ was reversed under the initially low PAR levels of increasing RLCs. As samples were  
225 subjected to increasing light intensity,  $F_m'$  decreased steadily to  $84 \pm 23.2\%$  of initial values  
226 due to NPQ induction, whilst  $F'$  returned to approximately initial values ( $103 \pm 29.3\%$  of the

227 value in the dark). Conversely, both  $F'$  and  $F_m'$  slowly decreased below initial values  
228 (measured in the dark,  $F_o$  and  $F_m$ ) at the beginning of decreasing RLCs (Figure 5b), with  
229 decreases accelerating at light intensity less than ca.  $800 \mu\text{mol m}^{-2} \text{s}^{-1}$ , the point at which  
230 NPQ increased. With decreases in light intensity to  $140 \mu\text{mol m}^{-2} \text{s}^{-1}$ ,  $F'$  reduced to  $53 \pm$   
231  $9.9\%$  and  $F_m'$  to  $64 \pm 11.4\%$  of initial values. Note the slight increase in both  $F'$  and  $F_m'$   
232 when exposed to darkness at the end of decreasing RLCs (Figure 5b).

233 Monitoring of photochemistry during induction/recovery curves indicated a small  
234 amount of photoacclimation during the 400-second induction phase at  $803 \mu\text{mol m}^{-2} \text{s}^{-1}$ ,  
235 whereby initial declines in quantum efficiency from  $0.29 \pm 0.025$  to  $0.11 \pm 0.038$  at the onset  
236 of illumination were recovered to  $0.13 \pm 0.025$  by the end illumination (Figure 6). With the  
237 onset of the dark recovery phase, rapid increases in quantum efficiency to  $0.26 \pm 0.041$   
238 demonstrated almost full recovery to initial values. During the remainder of the recovery  
239 phase, quantum efficiency slowly increased to  $0.45 \pm 0.063$ , i.e. well above initial values,  
240 suggesting significant retention of down regulation in samples from exposure to ambient light  
241 prior to measurements. However, examination of the operational ( $F'$  or  $F$  in the induction and  
242 recovery phases, respectively) and maximum ( $F_m'$  or  $F_m$ , respectively) fluorescence yields  
243 (Figure 7) revealed unexpected patterns.  $F'$  initially increased during the induction phase,  
244 presumably due to ubiquinone Qa reduction (lack of increase in  $F_m'$  precluding NPQ  
245 relaxation), before decreasing as Qa oxidation (unlikely) and/or NPQ induction (most likely)  
246 occurred during the induction phase. After 400 seconds, decreases in  $F$  with the onset of the  
247 dark recovery phase, presumably reflecting Qa oxidation, outweighed the effects of NPQ  
248 reversal; however, continued decreases in  $F$  over the remainder of the recovery phase  
249 suggested continued NPQ induction in darkness. In a similar manner,  $F_m'$  decreased during  
250 the induction phase suggesting NPQ induction, showed a slight increase with the onset of the  
251 recovery phase, i.e. slight NPQ reversal, though subsequently declined over the remainder of

252 the recovery phase indicating continued NPQ induction in the dark. Increases in quantum  
253 efficiency during the recovery phase (Figure 6) were the result of a greater proportional  
254 decrease in  $F$  compared to  $F_m$  (Figure 7).

255

## 256 **Discussion**

257 Cryoconite phototrophs on Longyearbreen, Svalbard demonstrated a high capability  
258 for rapid photoacclimation, via a combination of behavioural and physiological down  
259 regulation of photochemistry. The former involves a self-shading process, either chloroplast  
260 shading, cell positioning within the cryoconite sediment, or both processes. The latter appears  
261 to be a combination of two forms of non-photochemical quenching (NPQ), however this is  
262 complicated as a result of the mixed community due to employment of state changes by  
263 cyanobacteria which induce rapid changes in fluorescence yields in the same form as NPQ.  
264 Overall, there is a high plasticity of photoacclimation in cryoconite phototrophs, which ensures  
265 cells are ideally adapted to high light exposure on the ice surfaces in these high-stress polar  
266 environments.

267 The phototrophic communities of the three cryoconite holes investigated clearly  
268 differed despite being hydrologically connected. Pigment analysis indicated that all three  
269 holes showed the typical dominance of green algae and cyanophyta within cryoconite  
270 material (Langford *et al.*, 2011; Cameron *et al.*, 2012; Yallop *et al.*, 2012; Edwards *et al.*,  
271 2014), with only trace levels of fucoxanthin and hence low biomass of diatoms. Hole 1 was  
272 dominated by green algae, principally chlorophytes and streptophytes (indicated by high Chl  
273 b : Chl a ratio and the relatively high presence of lutein; streptophytes are closely related to  
274 Charophyceae and Embryophyta and hence have similar pigments), whereas holes 2 and 3  
275 were relatively more dominated by cyanobacteria. The cyanobacteria community also

276 differed between holes, based on the relative concentrations of echinenone and  
277 canthaxanthin, although all three holes had a high relative abundance of *Nostoc*. Interestingly,  
278 there were no significant differences in community measurements of photophysiology  
279 between the holes, despite the differences in phototrophic community structure.

280           Photophysiological data from rapid light curves and induction/recovery curves  
281 demonstrated a high plasticity of response, with several mechanisms of photoacclimation  
282 identified that allow the cryoconite phototrophic community to effectively photoacclimate to  
283 the high-light regime experienced *in situ*. Photoacclimation methods can be considered to be  
284 either physiological or behavioural (Perkins *et al.* 2002; 2010a,b; Lavaud and Goss 2015).  
285 Physiological photoacclimation refers largely to photochemical down regulation, including  
286 non-photochemical quenching (NPQ) in eukaryote phototrophs, whereby the light-driven de-  
287 epoxidation of specific xanthophyll pigments quenches excess excitation energy in the  
288 antennae complex as heat (Consalvey *et al.* 2005; Lavaud and Lepetit 2013). In  
289 cyanobacteria, state transitions to balance excitation between photosystems is also a form of  
290 physiological photochemical regulation (Campbell *et al.* 1998). Behavioural  
291 photoacclimation is largely cell motility as a response to changes in light environment,  
292 whereby cells move away from high light or towards low light in order to optimise their  
293 efficiency of photochemistry (Forster and Kromkamp 2004; Perkins *et al.* 2002; 2010a,b).  
294 However, Yallop *et al.* (2012) expanded upon this by hypothesising that ice algae used  
295 chloroplast movement to facilitate shading behind dark, tertiary pigments. Separation of the  
296 two processes through *in situ* measurements would be extremely difficult, if not impossible,  
297 hence we refer to behavioural down regulation as the likely composite of these two processes.  
298 We therefore hypothesise that cryoconite phototrophs utilise chloroplast movement and / or  
299 cell positioning in order to adjust to changing light environments. Such cell motility to  
300 facilitate shading within the cryoconite matrix likely explains why light curves with

301 increasing light increments failed to saturate, whereas decreasing light curves did saturate.  
302 Increasing curves provide enough time for chloroplast movement inside the cells and/or cell  
303 or filament movement in the sediment and hence the cells optimise their light environment.  
304 Phototrophic cryoconite communities are organised around granule structures, consisting of  
305 mineral grains, microorganisms and polymers (Takeuchi *et al.* 2001; Hodson *et al.* 2010;  
306 Langford *et al.* 2010; Segawa *et al.* 2014). This is analogous to microbial biofilms in fine  
307 sediments, where down regulation is achieved using a mixture of cell motility and NPQ  
308 (Perkins *et al.* 2010a,b; Lavaud and Goss 2015). In these systems, a lack of RLC saturation  
309 has been attributed to cell movement away from increasing light levels (Perkins *et al.* 2002;  
310 2010a,b). Cyanobacteria, green algae and diatoms are known to utilise cell motility to move  
311 away from high light and UV-stress through the process of microcycling and bulk migration  
312 (Bebout and Garcia-Pichel 1995; Kromkamp *et al.* 1998; Consalvey *et al.* 2004; Forster and  
313 Kromkamp 2004; Serôdio 2004; Perkins *et al.* 2002; 2010a,b). During the present study,  
314 microscopy and pigment profiles confirmed the presence of cyanobacteria, diatoms (at very  
315 low levels of abundance) and green algae in the cryoconite material, corroborating previous  
316 findings (Stibal *et al.* 2006; Yallop and Anesio 2010), and hence supporting the potential of  
317 cell motility as a means of down regulation. Cell movement within sediment is usually  
318 facilitated by extracellular polymer production (Consalvey *et al.* 2004), which is a well-  
319 reported characteristic of cryoconite granules (Langford *et al.* 2010; Zarsky *et al.* 2013;  
320 Segawa *et al.* 2014). Granules promote community stability (Hodson *et al.* 2010; Irvine-Fynn  
321 *et al.* 2011; Langford *et al.* 2014; Bagshaw *et al.* 2016b), and as we now reveal, also play a  
322 role in behavioural photoacclimation, Aggregation of cryoconite into granules thus enhances  
323 community production, by supporting a stable, cooperative microbial community, enabling  
324 physical migration to cope with the extreme glacier surface environment.

325 Behavioural down regulation of photochemistry (chloroplast movement and / or cell  
326 positioning within the sediment) has therefore been demonstrated for cryoconite phototrophic  
327 communities, but what is the role of physiological down regulation (in the form of NPQ in  
328 green algae and diatoms and state transitions in cyanobacteria) for these phototrophs?  
329 Calculation of NPQ from the change in maximum fluorescence yield during increasing  
330 incremental RLCs, indicated an initial reversal of NPQ retained from exposure to ambient  
331 light prior to measurements, highlighting NPQ as an important mechanism of down-  
332 regulation employed by cryoconite communities in situ. The subsequent slow induction of  
333 NPQ to values of around 0.5 during increasing RLCs further suggested this form of down-  
334 regulation to be applied proportionally to irradiance, as is a commonly held assumption  
335 underlying NPQ dynamics in microalgae (e.g. Lavaud and Goss 2014). However, by  
336 extending our assessment to include both decreasing light curves and induction/recovery  
337 curves, we were able to demonstrate unique features in the dynamics of cryoconite  
338 community down regulation that would not have been ascertainable using the commonly-  
339 applied increasing light curve technique alone. Firstly, contrasting dynamics in down-  
340 regulation during increasing and decreasing light curves indicated that behavioural, as  
341 opposed to physiological, down-regulation may form the major photo-acclimation  
342 mechanism employed in cryoconite holes on Svalbard glaciers. This would be in agreement  
343 for observations on sediment biofilm communities in intertidal estuaries (Perkins et al.  
344 2010a,b; Cartaxana et al. 2011). This is evidenced by the six-fold higher induction of NPQ  
345 apparent during decreasing as compared to increasing light curves, although the true  
346 magnitude difference in NPQ induction should not be directly compared, due to the  
347 differential levels of cell movement hypothesised. Cell movement to induce shading would  
348 result in a decrease in  $F_m'$  yield as well as that observed due to induction of NPQ (Forster and  
349 Kromkamp, 2004, Perkins et al., 2010), thus confounding the measurement of NPQ based on

350 change in maximum fluorescence yield (see Methods). Thus high NPQ could in fact be the  
351 sum of true NPQ induction and cell movement both reducing  $F_m'$  yield. However it is highly  
352 likely that the observed patterns in NPQ are indeed primarily physiological down regulation  
353 (energy dependent down regulation in eukaryote microalgae, but also state transitions in  
354 cyanobacteria, see below), at least in decreasing RLCs due to the timing and rate of  
355 induction. As well as demonstrating the significantly higher capacity for NPQ available to  
356 cryoconite phototrophs than estimated from increasing light curves, these trends provide  
357 insight into the likely balance between behavioural and physiological down-regulation  
358 employed in situ. During increasing light curves, it is likely that chloroplast movement and/or  
359 cell positioning in the sediment matrix, i.e. behavioural down-regulation, reduced the light  
360 stress experienced by cells, therefore reducing the requirement to induce NPQ. In contrast,  
361 the initial high light stress experienced during decreasing curves, coupled with the lack of  
362 time for chloroplast movement and/or cell positioning, resulted in cells inducing  
363 physiological down-regulation, i.e. NPQ, as a means to balance the irradiance provided. By  
364 comparing the magnitude of NPQ induced with/without the presence of behavioural down  
365 regulation, data indicate that the latter may account for ca. 75 % of the total down-regulation  
366 employed in cryoconite holes. In eukaryote microalgae this may be an adaptation to reduce  
367 the metabolic costs associated with production and inter-conversion of NPQ-associated  
368 pigments (Lavaud and Goss 2014) in this high-light environment. Secondly, the contrasting  
369 dynamics in down-regulation observed during the present study strongly indicated that  
370 additional to a combination of behavioural and typical physiological forms of down  
371 regulation, the cryoconite phototrophic communities further possess a rapidly induced, time  
372 or light-dose dependent form of NPQ, as opposed to primarily light intensity driven forms.  
373 With the onset of decreasing light curves, an initial slow level of NPQ was induced, followed  
374 by a more rapid induction at light levels below  $800 \mu\text{mol m}^{-2} \text{s}^{-1}$  PAR. This would parallel the



375 different forms of NPQ reported for diatoms (Lavaud and Goss 2014), although diatoms were  
376 observed to have extremely low abundance in the cryoconite. Rapidly induced energy  
377 dependent down regulation of this form, which is not reversed in darkness has been reported  
378 (Lavaud and Lepetit 2013) and referred to as photoinhibitory quenching (qI) or saturating  
379 NPQ (NPQs). NPQ was induced rapidly during our experiment, despite decreasing light  
380 levels, and was also retained in the dark. Such trends were also apparent during the dark  
381 recovery phase of induction/recovery curves. Examination of the fluorescence yields showed  
382 that both  $F$  and  $F_m$  initially increased in the dark recovery phase, presumably due to NPQ  
383 reversal, but then declined despite the increase in dark quantum efficiency ( $F_v/F_m$ ) observed.  
384 There would therefore appear to be either a time or potentially light-dose dependent form of  
385 physiological down-regulation that, once triggered, does not decrease with decreasing PAR,  
386 nor is rapidly (i.e. within the duration of dark recovery employed here) reversed in the dark.

387         It is important to note that our measurements were made on a mixed community  
388 largely dominated by green algae and cyanobacteria. The latter appear not to have energy  
389 dependent NPQ but rapid changes in fluorescence are observed through state transitions  
390 utilising phycobilosome diffusion (Campbell and Oquist 1996, Campbell et al. 1998). This  
391 form of rapid down regulation would result in similar changes in fluorescent yields as NPQ in  
392 green algae, e.g. a quenching as light increased followed by reversal in darkness. During  
393 increasing rapid light curves, state transitions (state 2 to state 1) would result in a decrease in  
394  $F_m'$  and hence an increase in our measured NPQ, however shading processes through cell  
395 motility described above would negate the need for this down regulation in increasing RLCs.  
396 In decreasing light curves, state 2 to state 1 transition would be induced in cyanobacteria at  
397 the same time as energy dependent NPQ would be induced in the eukaryote microalgae. It  
398 may be that as light levels reduced in these decreasing RLCs, the induction of this state  
399 transition was not reversed increasing the relative level of quenching and hence the large

400 increase in measured NPQ. Obviously it would not be possible to differentiate between the  
401 two processes in such a mixed community using in situ fluorescence measurements, however  
402 we suggest that there is a high likelihood of physiological down regulation employed by both  
403 the eukaryote microalgae (energy dependent down regulation) and cyanobacteria (state  
404 transitions).

405         The combination of chloroplast movement, cell positioning and physiological down  
406 regulation by the cryoconite phototrophs is a highly efficient method of light acclimation that  
407 has serious implications for the interpretation of fluorescence based assessments of  
408 productivity. Specifically, the lack of saturation of light curves with increasing light  
409 increments indicates caution is required when utilising fluorescence on cryoconite.  
410 Productivity ( $rETR_{max}$ ) can clearly be significantly over-estimated when photoacclimation  
411 during the light curve occurs, whether this is through cell movement or chloroplast shading.  
412 In this study, the first steps of the RLC appear to be relatively unaffected, with  $\alpha$  similar for  
413 increasing and decreasing RLCs. However, as the light curves progressed, divergence  
414 between the curves showed an overestimation of  $rETR_{max}$  of over 100%, with similar over-  
415 estimation likely for light saturation parameters  $E_s$  and  $E_k$ . This should be corrected for in  
416 studies using fluorescence in order to avoid overestimation of productivity, and potentially  
417 the role of cryoconite phototrophs in carbon flux calculations (Hodson *et al.* 2007; Anesio *et*  
418 *al.* 2010; Cook *et al.* 2012; Chandler *et al.* 2015; Bagshaw *et al.* 2016a).

419         In conclusion, this study demonstrates that the phototrophic cryoconite community on  
420 Longyearbreen, Svalbard, utilise a mixture of behavioural and physiological (likely a mixture  
421 of non-photochemical quenching in eukaryotes and state transitions in cyanobacteria) down  
422 regulation of photochemistry. Cells appear to be capable of optimising their light  
423 environment through chloroplast shading and/or cell positioning within the cryoconite,  
424 effectively behavioural down regulation. Shading through chloroplast movement and cell

425 positioning is likely to result in an overestimation of productivity when using increasing  
426 incremental rapid light curves. In future work this may be corrected for by using the product  
427 of ETR and the operational fluorescence  $F'$  (Ihnken et al. 2014), however this was tested in  
428 this study and did not alter the shape of the RLCs. In the cryoconite studied here, the  
429 phototrophs, primarily a mixture of green algae and two different cyanophyte communities,  
430 showed high plasticity of photophysiology, indicating extremely high capability for light  
431 acclimation. This would be expected for cells inhabiting polar ice surfaces, where light  
432 intensity and light dose can be high and fluctuate quickly. Aggregation of cryoconite into  
433 granules is therefore an important adaptation which not only prolongs microbial community  
434 stability, but also allows light acclimation and hence promotes ecosystem productivity.

435

#### 436 **Acknowledgements**

437 RP was funded by a British Phycological Society Small Project Grant. LM had combined  
438 funding from Royal Geography Society Small Research Grant, Geological Society of London  
439 Robert Scott Memorial Award and Forskningsradet Norge, Arctic Field Grant no 246072.  
440 The work was carried out on Research Project RiS 10281. MLY was supported by a  
441 Leverhulme Research Fellowship RF 2014-708. We should also like to thank the two  
442 anonymous reviewers for their highly constructive reviews.

443

444 **References**

- 445 Anesio, AM., Sattler, B, Foreman, CM., Telling, J, Hodson, A, Tranter, M and Psenner, R.  
446 Carbon Fluxes through Bacterial Communities on Glacier Surfaces. *Annals of Glaciology*  
447 2010; 51(56): 32-40
- 448 Bagshaw, EA, Tranter, M, Fountain, AG, Welch, K, Basagic, HJ and Lyons, WB . Do  
449 Cryoconite Holes Have the Potential to Be Significant Sources of C, N, and P to Downstream  
450 Depauperate. *Arctic Antarctic and Alpine Research* 2013; 45(4): 440-454 doi: 10.1657/1938-  
451 4246-45.4.440
- 452 Bagshaw, EA, Tranter, M, Wadham, J, Fountain, AG, Dubnick, A and Fitzsimons, S .  
453 Processes Controlling Carbon Cycling in Antarctic Glacier Surface Ecosystems. *Geochemical*  
454 *Perspectives Letters* 2016a; In Press
- 455 Bagshaw, EA, Tranter, M, Wadham, JL, Fountain, AG and Basagic, H. Dynamic Behaviour  
456 of Supraglacial Lakes on Cold Polar Glaciers: Canada Glacier, Mcmurdo Dry Valleys,  
457 Antarctica. *Journal of Glaciology* 2010; 56(196): 366-368
- 458 Bagshaw, EA, Wadham, JL, Tranter, M, Perkins, R, Morgan, A, Williamson, CJ, Fountain,  
459 AG, Fitzsimons, S and Dubnick, A. Response of Antarctic Cryoconite Microbial  
460 Communities to Light. *Fems Microbiology Ecology* 2016b; 92(6) doi:  
461 10.1093/femsec/fiw076
- 462 Bebout, BM, and Garcia-Pichel F. UVB-induced vertical migrations of cyanobacteria in a  
463 microbial mat. *Applied and Environmental Microbiology* 1995; 61: 4215-4222.
- 464 Benning, LG, Anesio, AM, Lutz, S and Tranter, M. Biological Impact on Greenland's  
465 Albedo. *Nature Geoscience* 2014; 7(10): 691-691
- 466 Campbell, D, Öquist, G. Predicting Light Acclimation in Cyanobacteria from  
467 Nonphotochemical Quenching of Photosystem I I Fluorescence, Which Reflects State  
468 Transitions in These Organisms. *Plant Physiol.* (1996) 11 1: 1293-1298
- 469 Campbell, D, Hurry, V, Clarke, AK, Gustafsson, Öquist, G. Chlorophyll fluorescence  
470 analysis of cyanobacterial photosynthesis and acclimation. *Microbiol Mol Biol Rev.* 1998:  
471 62(3):667-83
- 472

473  
474 Cameron, KA, Hodson, AJ and Osborn, AM. Structure and Diversity of Bacterial, Eukaryotic  
475 and Archaeal Communities in Glacial Cryoconite Holes from the Arctic and the Antarctic.  
476 *Fems Microbiology Ecology* 2012; 82(2): 254-267 doi: 10.1111/j.1574-6941.2011.01277.x

477 Cartaxana, P, Ruivo, M, Hubas, C, Davidson, I, Serôdio, J, Jesus, B. Light and O<sub>2</sub>  
478 microenvironments in two contrasting diatom-dominated coastal sediments. *Mar. Ecol. Prog.  
479 Ser.* 2011; 545: 35-47

480 Chandler, DM, Alcock, JD, Wadham, JL, Mackie, SL and Telling, J. Seasonal Changes of Ice  
481 Surface Characteristics and Productivity in the Ablation Zone of the Greenland Ice Sheet.  
482 *Cryosphere* 2015; 9(2): 487-504 doi: 10.5194/tc-9-487-2015

483 Consalvey MC, Jesus B, Perkins RG, Brotas V, Underwood GJC, Paterson DM. Monitoring  
484 migration and measuring biomass in benthic biofilms: the effects of dark/far-red adaptation  
485 and vertical migration on fluorescence measurements. *Photosynth Res.* 2004; 81:91–101

486 Consalvey, MC, Perkins RG, Paterson DM, Underwood GJC. PAM Fluorescence: A  
487 beginners guide for benthic diatomists. *Diatom Res.* 2005; 20:1–22

488 Cook, JM, Hodson, AJ, Anesio, AM, Hanna, E, Yallop, M, Stibal, M, Telling, J and  
489 Huybrechts, P. An Improved Estimate of Microbially Mediated Carbon Fluxes from the  
490 Greenland Ice Sheet. *Journal of Glaciology* 2012; 58(212): 1098-1108 doi:  
491 10.3189/2012JoG12J001

492 Dieser, M, Greenwood, M and Foreman, CM. Carotenoid Pigmentation in Antarctic  
493 Heterotrophic Bacteria as a Strategy to Withstand Environmental Stresses. *Arctic Antarctic  
494 and Alpine Research* 2010; 42(4): 396-405 doi: 10.1657/1938-4246-42.4.396

495 Edwards, A, Mur, LAJ, Girdwood, SE, Anesio, AM, Stibal, M, Rassner, SME, Hell, K,  
496 Pachebat, JA, Post, B, Bussell, JS, Cameron, SJS, Griffith, GW, Hodson, AJ and Sattler, B.  
497 Coupled Cryoconite Ecosystem Structure-Function Relationships Are Revealed by  
498 Comparing Bacterial Communities in Alpine and Arctic Glaciers. *Fems Microbiology  
499 Ecology* 2014; 89(2): 222-237 doi: 10.1111/1574-6941.12283

500 Etzelmüller, B, Schuler, TV, Isaksen, K, Christiansen, HH, Farbro, H and Benestad, R.  
501 Modeling the temperature evolution of Svalbard permafrost during the 20th and 21st century.  
502 *The Cryosphere* 2011; 5, 67–79.

503 Forster, RM, Kromkamp, JC. Modelling the effects of chlorophyll fluorescence from  
504 subsurface layers on photosynthetic efficiency measurement in microphytobenthic algae.  
505 Marine Ecology-Progress Series 2004; 284:9-22

506 Foreman, CM, Wolf, CF and Priscu, JC. Impact of Episodic Warming Events on the Physical,  
507 Chemical and Biological Relationships of Lakes in the McMurdo Dry Valleys, Antarctica.  
508 Aquatic Geochemistry 2004; 10(3): 239-268

509 Hammer, Ø, Harper, DAT, and Ryan, PD. PAST: Paleontological Statistics Software  
510 Package for Education and Data Analysis. Palaeontologia Electronica 2001; 4(1): 9pp.

511 Hodson, A, Anesio, AM, Ng, F, Watson, R, Quirk, J, Irvine-Fynn, T, Dye, A, Clark, C,  
512 McCloy, P, Kohler, J and Sattler, B. A Glacier Respires: Quantifying the Distribution and  
513 Respiration Co<sub>2</sub> Flux of Cryoconite across an Entire Arctic Supraglacial Ecosystem. Journal  
514 of Geophysical Research-Biogeosciences 2007; 112(G4) doi: G04s3610.1029/2007jg000452

515 Hodson, A, Cameron, K, Boggild, C, Irvine-Fynn, T, Langford, H, Pearce, D and Banwart, S.  
516 The Structure, Biological Activity and Biogeochemistry of Cryoconite Aggregates Upon an  
517 Arctic Valley Glacier: Longyearbreen, Svalbard. Journal of Glaciology 2010; 56(196): 349-  
518 362

519 Ihnken S, Kromkamp J, Beardall J, Silsbe G. State-transitions facilitate robust quantum yields  
520 and cause an over-estimation of electron transport in *Dunaliella tertiolecta* cells held at the  
521 CO<sub>2</sub> compensation point and re-supplied with DIC. Photosynthesis Research 2014; 119:257-  
522 272

523 Irvine-Fynn, TDL, Bridge, JW and Hodson, AJ. In Situ Quantification of Supraglacial  
524 Cryoconite Morphodynamics Using Time-Lapse Imaging: An Example from Svalbard.  
525 Journal of Glaciology 2011; 57(204): 651-657

526 Kaczmarek, L, Jakubowska, N, Celewicz-Goldyn, S and Zawierucha, K. The  
527 Microorganisms of Cryoconite Holes (Algae, Archaea, Bacteria, Cyanobacteria, Fungi, and  
528 Protista): A Review. Polar Record 2016; 52(2): 176-203 doi: 10.1017/s0032247415000637

529 Kromkamp J, Barranguet C, Peene J. Determination of microphytobenthos PSII quantum  
530 efficiency and photosynthetic activity by means of variable chlorophyll fluorescence. Mar.  
531 Ecol. Prog. Ser. 1998; 162:45–55

532 Larsson, S. Geomorphological effects on the slopes of Longyear Valley, Spitsbergen, after a  
533 heavy rainstorm in July 1972. *Geogr. Ann.* 1982; 64A: 105 - 125

534 Langford, HJ, Hodson, A and Banwart, S. Using Ftir Spectroscopy to Characterise the Soil  
535 Mineralogy and Geochemistry of Cryoconite from Aldegondabreen Glacier, Svalbard.  
536 *Applied Geochemistry* 2011; 26: S206-S209 doi: 10.1016/j.apgeochem.2011.03.105

537 Langford, HJ, Hodson, A, Banwart, S and Boggild, C. The Microstructure and  
538 Biogeochemistry of Arctic Cryoconite Granules. *Annals of Glaciology* 2010; 51(56): 87-94

539 Langford, HJ, Irvine-Fynn, TDL, Edwards, A, Banwart, SA and Hodson, AJ. A Spatial  
540 Investigation of the Environmental Controls over Cryoconite Aggregation on Longyearbreen  
541 Glacier, Svalbard. *Biogeosciences* 2014; 11(19): 5365-5380 doi: 10.5194/bg-11-5365-2014

542 Lavaud, J and Goss, R. The Peculiar Features of Non-Photochemical Fluorescence  
543 Quenching in Diatoms and Brown Algae. *Advances in Photosynthesis and Respiration* 2014;  
544 40: 421-443

545 Lavaud, J and Lepetit, B. An explanation for the inter-species variability of the  
546 photoprotective and non-photochemical chlorophyll fluorescence quenching in diatoms.  
547 *Biochim. Biophys. Acta* 2013; 1827: 294-302

548 Lawson, EC, Wadham, JL, Tranter, M, Stibal, M, Lis, GP, Butler, CEH, Laybourn-Parry, J,  
549 Nienow, P, Chandler, D and Dewsbury, P. Greenland Ice Sheet Exports Labile Organic  
550 Carbon to the Arctic Oceans. *Biogeosciences* 2014; 11(14): 4015-4028 doi: 10.5194/bg-11-  
551 4015-2014

552 Lutz, S, Anesio, AM, Villar, SEJ. and Benning, LG. Variations of Algal Communities Cause  
553 Darkening of a Greenland Glacier. *Fems Microbiology Ecology* 2014; 89(2): 402-414 doi:  
554 10.1111/1574-6941.12351

555 McMinn A, Ryan KG, Ralph P, Pankowski A. Spring sea ice photosynthesis, primary  
556 productivity and biomass distribution in eastern Antarctica, 2002–2004. *Mar. Biol.* 2007;  
557 151:985–995

558 Musilova, M, Tranter, M, Bamber, JL, Takeuchi, N and Anesio, A. Experimental Evidence  
559 That Microbial Activity Lowers the Albedo of Glaciers. *Geochemical Perspectives Letters*  
560 2016; 2(0): 106-116 oi: <http://dx.doi.org/10.7185/geochemlet.1611>

561 Perkins, RG , Oxborough, K, Hanlon, ARM, Underwood, GJC and Baker, NR. Can  
562 chlorophyll fluorescence be used to estimate the rate of photosynthetic electron transport  
563 within microphytobenthic biofilms? *Mar. Ecol. Prog. Ser.* 2002; 228: 47 - 56

564 Perkins, RG, Mouget, J-L, Lefebvre, S and Lavaud, J. Light response curve methodology and  
565 possible implications in the application of chlorophyll fluorescence to benthic diatoms. *Mar.*  
566 *Biol.* 2006; 149: 703 - 712.

567 Perkins, RG, Kromkamp. JC, Serôdio, J, Lavaud, J, Jesus, B, Mouget, J-L, Lefebvre, S,  
568 Forster, RM. The application of variable chlorophyll fluorescence to microphytobenthic  
569 biofilms. In *Chlorophyll a fluorescence in aquatic sciences: methods and applications*, Edited  
570 by Suggett, D., Prasil O., & Borowitzka M. *Developments in Applied Phycology 2010a*; Vol  
571 4: 237-275. Springer, UK. ISBN 978-90-481-9267-0.

572 Perkins, RG, Lavaud, J, Serôdio, J, Mouget, J-L, Cartaxana, P, Rosa, P, Barille, L, Brotas, V,  
573 Jesus, BM. Vertical cell movement is a primary response of intertidal benthic biofilms to  
574 increasing light dose. *Mar. Ecol. Prog. Ser.* 2010b; 16: 93-103

575 Remias, D, Pichrtová, M, Pangratz, M, Lütz, C and Holzinger, A. Secondary Pigments and  
576 Ultrastructure of *Chlainomonas* Sp. (Chlorophyta) from the European Alps Compared with  
577 *Chlamydomonas Nivalis* Forming Red Snow. *Fems Microbiology Ecology* 2016; 92(4) doi:  
578 10.1093/femsec/fiw030

579 Segawa, T, Ishii, S, Ohte, N, Akiyoshi, A, Yamada, A, Maruyama, F, Li, ZQ, Hongoh, Y and  
580 Takeuchi, N. The Nitrogen Cycle in Cryoconites: Naturally Occurring Nitrification-  
581 Denitrification Granules on a Glacier. *Environmental Microbiology* 2014; 16(10): 3250-3262  
582 doi: 10.1111/1462-2920.12543

583 Serôdio J. Analysis of variable chlorophyll fluorescence in microphytobenthos assemblages:  
584 implications of the use of depth-integrated measurements. *Aquat Microb Ecol* 2004; 36:137-  
585 152

586 Stibal, M, Elster, J, Šabacká, M and Kaštovská, K. Seasonal and Diel Changes in  
587 Photosynthetic Activity of the Snow Alga *Chlamydomonas Nivalis* (Chlorophyceae) from  
588 Svalbard Determined by Pulse Amplitude Modulation Fluorometry. *Fems Microbiology*  
589 *Ecology* 2007; 59(2): 265-273 doi: 10.1111/j.1574-6941.2006.00264.x



590 Stibal, M, Sabacka, M and Kastovska, K. Microbial Communities on Glacier Surfaces in  
591 Svalbard: Impact of Physical and Chemical Properties on Abundance and Structure of  
592 Cyanobacteria and Algae. *Microbial Ecology* 2006; 52(4): 644-654

593 Takeuchi, N. Optical Characteristics of Cryoconite (Surface Dust) on Glaciers: The  
594 Relationship between Light Absorbency and the Property of Organic Matter Contained in the  
595 Cryoconite. *Annals of Glaciology* 2002a; 32: 409-414

596 Takeuchi, N. Surface Albedo and Characteristics of Cryoconite (Biogenic Dust) on an  
597 Alaskan Glacier, Gulkana in the Alaska Range. *Bulletin of Glaciological Research* 2002b; 19:  
598 63-70

599 Takeuchi, N, Kohshima, S and Seko, K. Structure, Formation, and Darkening Process of  
600 Albedo-Reducing Material (Cryoconite) on a Himalayan Glacier: A Granular Algal Mat  
601 Growing on the Glacier. *Arctic Antarctic and Alpine Research* 2001; 33(2): 115-122

602 Tedesco, M, Doherty, S, Fettweis, X, Alexander, P, Jeyaratnam, J and Stroeve, J. The  
603 Darkening of the Greenland Ice Sheet: Trends, Drivers, and Projections (1981-2100).  
604 *Cryosphere* 2016; 10(2): 477-496 doi: 10.5194/tc-10-477-2016

605 Van Heukelem, L and Thomas, CS. Computer-assisted high-performance liquid  
606 chromatography method development with applications to the isolation and analysis of  
607 phytoplankton pigments. *Journal of Chromatography A* 2010; 910: 31 49

608 Yallop, ML and Anesio, AM. Benthic Diatom Flora in Supraglacial Habitats: A Generic-  
609 Level Comparison. *Annals of Glaciology* 2010; 51(56): 15-22 doi:  
610 10.3189/172756411795932029

611 Yallop, ML, Anesio, AM, Perkins, RG, Cook, J, Telling, J, Fagan, D, MacFarlane, J, Stibal,  
612 M, Barker, G, Bellas, C, Hodson, A, Tranter, M, Wadham, J and Roberts, NW.  
613 Photophysiology and Albedo-Changing Potential of the Ice Algal Community on the Surface  
614 of the Greenland Ice Sheet. *Isme Journal* 2012; 6(12): 2302-2313 doi:  
615 10.1038/ismej.2012.107

616 Zarsky, JD, Stibal, M, Hodson, A, Sattler, B, Schostag, M, Hansen, LH, Jacobsen, CS and  
617 Psenner, R. Large Cryoconite Aggregates on a Svalbard Glacier Support a Diverse Microbial  
618 Community Including Ammonia-Oxidizing Archaea. *Environmental Research Letters* 2013;  
619 8(3) doi: 10.1088/1748-9326/8/3/035044

620 Zawierucha, K, Kolicka, M, Takeuchi, N and Kaczmarek, L. What Animals Can Live in  
621 Cryoconite Holes? A Faunal Review. *Journal of Zoology* 2015; 295(3): 159-169 doi:  
622 10.1111/jzo.12195

623

624

625 **Table 1.** Species Composition of Cryoconite Material (pooled for three cryoconite holes)

626

<u>Cyanophyta</u>	Chlorophyta	Streptophyta	Chromophyta
<i>Leptolyngbya</i> spp.	<i>Chlamydomonas</i> cf. <i>nivalis</i>	<i>Ancylonema</i> <i>nordenskiöldii</i>	Pennate diatom spp.
<i>Nostoc</i> spp.	<i>Chlamydomonas</i> spp.	<i>Cylindrocystis</i> <i>brebissonii</i>	
<i>Oscillatoria</i> spp.		<i>Mesotaenium</i> <i>berggrenii</i>	
<i>Pseudoanabaena</i> spp.			

627

628

629

630 **Table 2.** Concentration of pigments quantified in by HPLC. Values are given as  $\mu\text{g}\cdot\text{g}^{-1}$   
631 freeze-dried cryoconite material.

632

	<b>Hole 1</b>	<b>Hole 2</b>	<b>Hole 3</b>
<b>FUCO</b> <b>(Fucoxanthin)</b>	0.0464	0.0000	0.0513
<b>NEOX</b> <b>(Neoxanthin)</b>	0.0917	0.0000	0.0227
<b>VX</b> <b>(Violaxanthin)</b>	0.1180	0.0141	0.0408
<b>DDX</b> <b>(Diadinoxanthin)</b>	0.0602	0.0275	0.0250
<b>ZX (Zeaxanthin)</b>	0.0543	0.0000	0.0000
<b>LUT (Lutein)</b>	0.6769	0.0176	0.0635
<b>CANT</b> <b>(Canthaxanthin)</b>	0.4924	1.1182	0.6538
<b>CHLB</b> <b>(Chlorophyll b)</b>	1.3474	0.4198	0.0801
<b>ECHI</b> <b>(Echinenone)</b>	0.6267	0.1702	0.2387
<b>CHLA</b> <b>(Chlorophyll a)</b>	10.6670	6.1472	5.4459
<b>CART</b> <b>(Carotenoids)</b>	0.3431	0.0000	0.0622

633

634

635

636

637 **Table 3.** Pigment ratios relative to Chlorophyll a. For abbreviations, see Table 2.

638

	<b>Site 1</b>	<b>Site 2</b>	<b>Site 3</b>
<b>FUCO</b>	0.0044	0.0000	0.0094
<b>NEOX</b>	0.0086	0.0000	0.0042
<b>VX</b>	0.0111	0.0023	0.0075
<b>DDX</b>	0.0056	0.0045	0.0046
<b>ZX</b>	0.0051	0.0000	0.0000
<b>LUT</b>	0.0635	0.0029	0.0117
<b>CANT</b>	0.0462	0.1819	0.1200
<b>CHLB</b>	0.1263	0.0683	0.0147
<b>ECHI</b>	0.0588	0.0277	0.0438
<b>CART</b>	0.0322	0.0000	0.0114

639

640



641

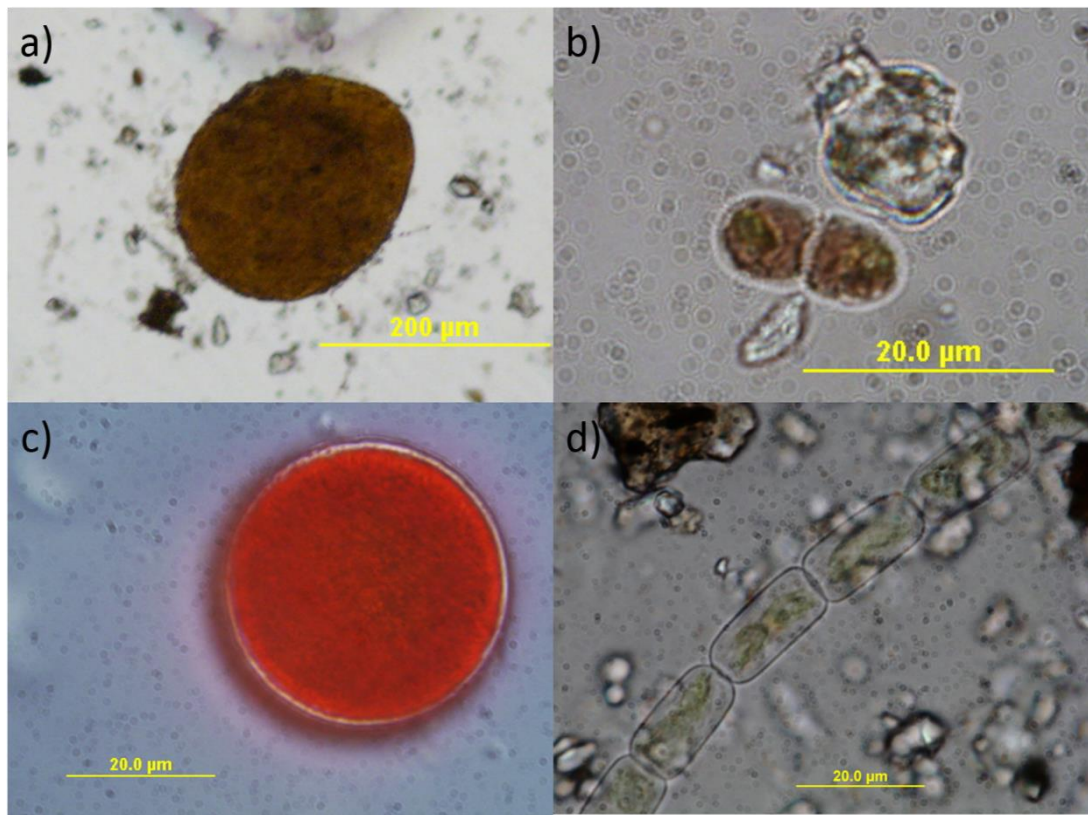
642

643 Figure 1. Location of sampling and *in situ* fluorescence measurements (blue dot) on the surface  
644 of Longyearbreen, Spitsbergen, Svalbard. Samples were collected from clean ice with  
645 intermittent cryoconite coverage, away from adjacent to areas with high concentrations of  
646 surface debris (upper insert, lower blue triangle) and meltwater channels (lower insert, upper  
647 blue triangle).

648

649

650



651

652

653

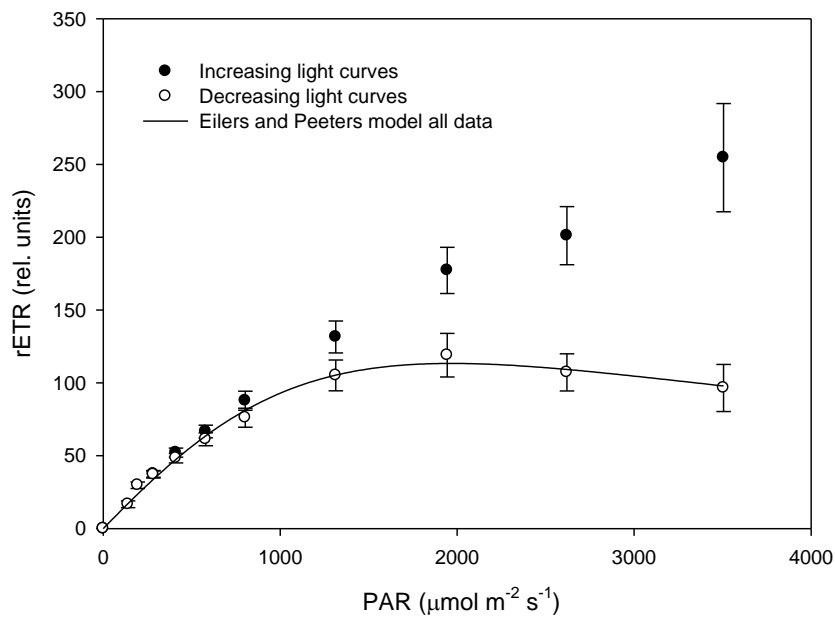
654 Figure 2. Cyanobacteria and algae from Longyearbreen cryconite: a) *Nostoc* sp. colony; b)  
655 Dividing cells of *Mesotaenium berggrenii*; c) Zygospore of *Chlamydomonas* cf. *nivalis*; d)  
656 Filament of *Ancydonema nordenskioldii*.

657

658

659

660



661

662

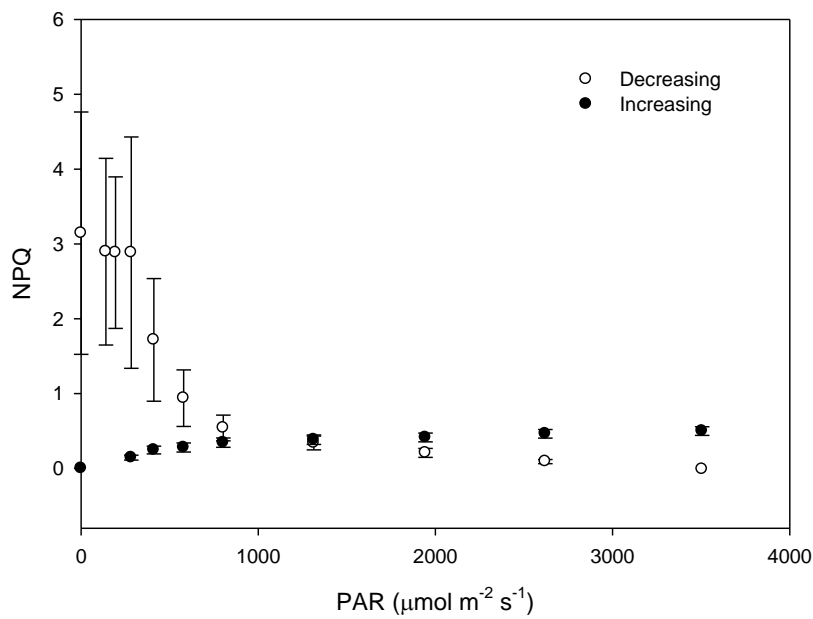
663 Figure 3. Increasing rapid light curve (RLC) data (closed symbols, mean  $\pm$  s.e., n = 15) showing no  
 664 saturation in comparison with decreasing RLC data (open symbols, mean  $\pm$  s.e., n = 15) showing  
 665 saturated light curves. Fitted line is the Eilers and Peeters (1988) model regressed to the 15 replicate  
 666 curves data points. Increasing and decreasing light curves were carried out on separate samples each  
 667 time and with sequentially increasing or decreasing light levels steps respectively.

668

669

670





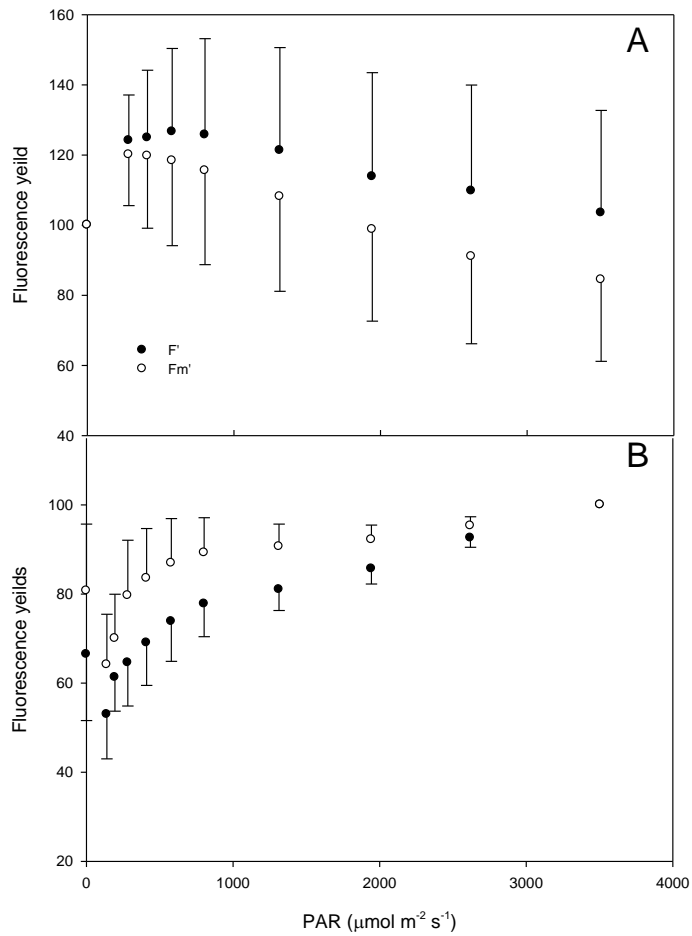
671

672 Figure 4. Increasing rapid light curve (RLC) non-photochemical quenching (NPQ) data (closed symbols,  
 673 mean  $\pm$  s.e., n = 15) and decreasing RLC NPQ data (open symbols, mean  $\pm$  s.e., n = 15) for the light  
 674 curves shown in Figure 3. Increasing and decreasing light curves were carried out on separate samples  
 675 each time and with sequentially increasing or decreasing light levels steps respectively.

676

677

678



679

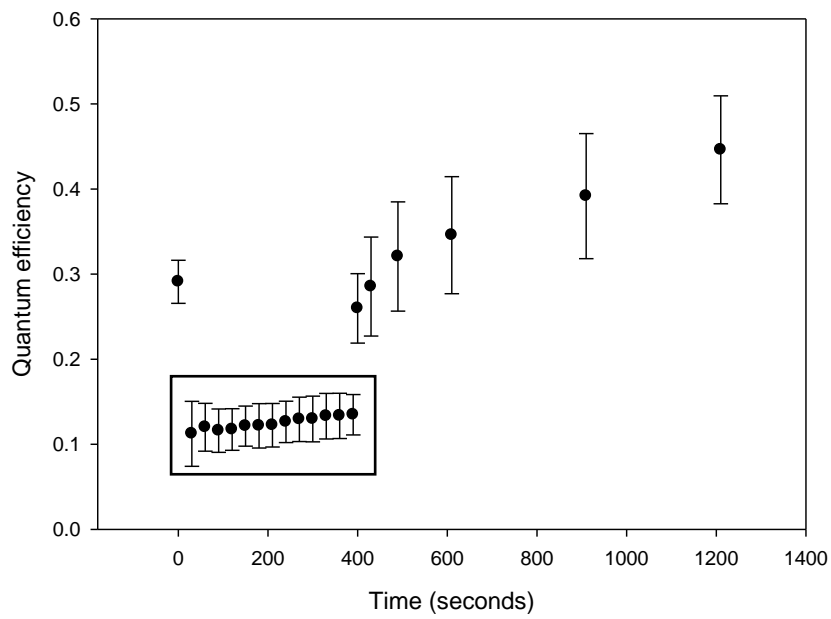
680

681 Figure 5. Operational fluorescence yield ( $F'$ , closed symbols) and maximum fluorescence yield ( $F_m'$ ,  
 682 open symbols) yield for increasing (a) and decreasing (b) rapid light curves shown in Figure 1 (both  
 683 data sets mean  $\pm$  s.e.,  $n = 15$ ). Data are represented as the percentage of the initial values obtained  
 684 from the first light curve step in each case (hence 100% at  $0 \mu\text{mol m}^{-2} \text{s}^{-1}$  for increasing and 100% at  
 685  $3,600 \mu\text{mol m}^{-2} \text{s}^{-1}$  PAR for decreasing light curve steps).

686

687

688



689

690

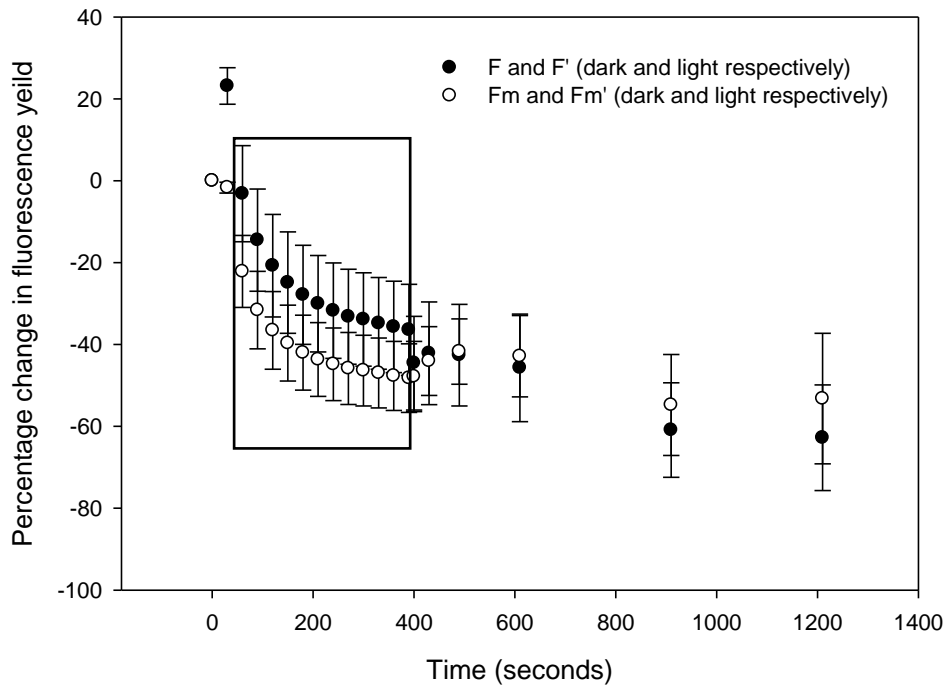
691 Figure 6. Quantum efficiency during induction recovery curve measurements (mean  $\pm$  s.e., n = 8). The  
 692 boxed area shows the efficiency during the induction phase with applied actinic light, other data points  
 693 are in darkness.

694

695

696

697



698

699 Figure 7. Percentage change, relative to initial values, of the operational fluorescence yield ( $F$  and  $F'$   
700 in the dark and light respectively) and maximum fluorescence yield ( $F_m$  and  $F_m'$  respectively) during  
701 induction recovery curves (mean  $\pm$  s.e.,  $n = 8$ ). The boxed area shows the yields measured during the  
702 induction phase with applied actinic light, other data points are in darkness.

703